

HyPER-GAN: Hybrid Patch-Based Image-to-Image Translation for Real-Time Photorealism Enhancement

Stefanos Pasios, Nikos Nikolaidis, *Senior Member, IEEE*

Abstract—Generative models are widely employed to enhance the photorealism of synthetic data for training computer vision algorithms. However, they often introduce visual artifacts that degrade the accuracy of these algorithms and require high computational resources, limiting their applicability in real-time training or evaluation scenarios. In this paper, we propose Hybrid Patch Enhanced Realism Generative Adversarial Network (HyPER-GAN), a lightweight image-to-image translation method based on a U-Net-style generator designed for real-time inference. The model is trained using paired synthetic and photorealism-enhanced images, complemented by a hybrid training strategy that incorporates matched patches from real-world data to improve visual realism and semantic consistency. Experimental results demonstrate that HyPER-GAN outperforms state-of-the-art paired image-to-image translation methods in terms of inference latency, visual realism, and semantic robustness. Moreover, it is illustrated that the proposed hybrid training strategy indeed improves visual quality and semantic consistency compared to training the model solely with paired synthetic and photorealism-enhanced images. Code and pretrained models are publicly available for download at: <https://github.com/stefanos50/HyPER-GAN>

Index Terms—Photorealism Enhancement, Image-to-Image Translation, Grand Theft Auto V, Computer Vision

I. INTRODUCTION

Synthetic visual data are widely utilized for training and evaluating computer vision algorithms in scenarios where real-world data collection is expensive, unsafe, or impractical. While modern simulation platforms [1]–[3] can generate large-scale visual datasets [4]–[6] with accurate annotations, the difference between the synthetic and real-world images, known as the appearance simulation-to-reality (sim2real) gap [7]–[9], often limits the real-world generalization performance of deep learning-based algorithms trained exclusively on synthetic data.

Image-to-image (Im2Im) translation [10] has emerged as the primary approach for reducing the appearance sim2real gap, as it can enhance the photorealism of synthetic images toward real-world characteristics while being less prone to visual artifacts (e.g., hallucinations) and significantly more computationally efficient than alternative generative approaches, such as diffusion models [11], [12] (see Appendix A). Im2Im translation methods can be categorized into unpaired [13]–[16] and paired [17]–[20] approaches, depending on whether pixel-aligned source–target image pairs depicting the same content

are available during training. For photorealism enhancement, unpaired Im2Im translation has been the dominant approach due to the practical difficulty of acquiring synthetic–real-world image pairs with pixel-level correspondences. Methods such as DCLGAN [14] illustrated promising results for photorealism enhancement [21]. More recent works proposed robust unpaired Im2Im translation approaches that further improved both visual fidelity and semantic consistency by utilizing additional inputs produced during synthetic image rendering, commonly referred to as G-Buffers (e.g., depth, surface normals, and semantic segmentation label maps) [7], [22], [23] that provide material, geometric, and semantic constraints and thus reduce the probability of generating artifacts (e.g., adding vegetation in the sky [22]). Since these G-Buffers require complex architectures that process them, these approaches are computationally expensive and slow at inference, running at 10 Frames Per Second (FPS) or below.

Due to the lack of paired synthetic and real-world images, paired Im2Im translation focused on photorealism enhancement by synthesizing real-world images from semantic segmentation ground-truth annotations generated in synthetic environments (e.g., video games) [24]. Considering that image synthesis is sensitive to the content distribution seen during training, this approach illustrated lower visual quality compared to the robust unpaired Im2Im translation methods [22]. To overcome the computational limitations of robust unpaired Im2Im translation methods that process additional information (i.e., G-Buffers) through complex deep learning architectures, the most recent paired Im2Im translation approach, REGEN [18], reformulated the paired Im2Im translation strategy for photorealism enhancement. The reformulation involved the use of outputs from a robust unpaired Im2Im model [22] as proxy pairs for the real-world domain to regenerate the results with improved inference speed and without requiring the additional G-Buffers. However, the FPS achieved remained below real-time performance (30 FPS) at high resolutions (e.g., 1080p), and the framework could not reach or surpass the semantic robustness of the initial robust unpaired Im2Im model, particularly due to the lack of an additional mechanism for avoiding learning the failure cases (artifacts) that can be potentially produced during the unpaired Im2Im translation phase [15].

In this work, we build upon the paired Im2Im concept introduced by REGEN and propose *Hybrid Patch Enhanced Realism Generative Adversarial Network (HyPER-GAN)*, a lightweight method designed for real-time photorealism en-

The authors are with the School of Informatics, Aristotle University of Thessaloniki, Thessaloniki 54124, Greece (email: {pstefanos,nnik}@csd.auth.gr).

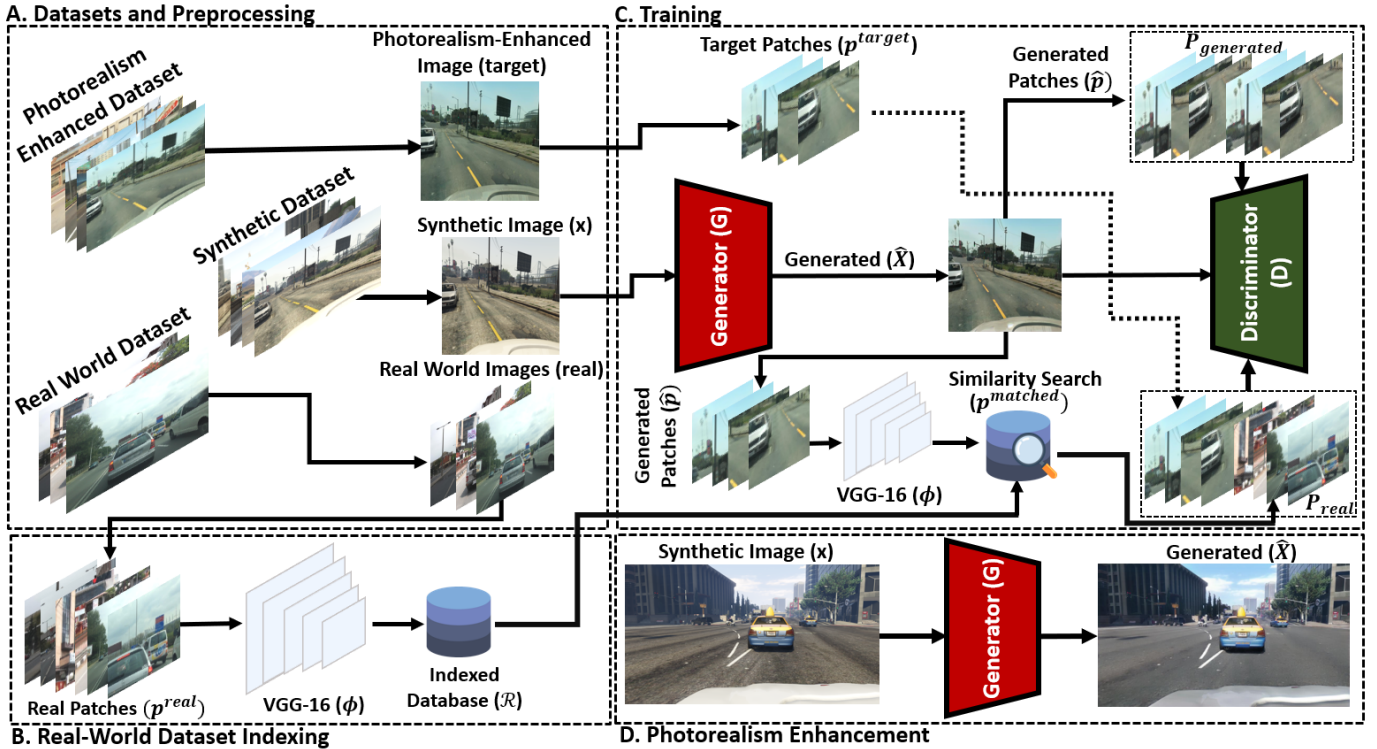


Fig. 1. Overview of the HyPER-GAN method, which includes four phases: a) datasets and preprocessing, b) real-world dataset indexing, c) training, and d) photorealism enhancement.

hancement of synthetic images. In detail, HyPER-GAN employs a compact U-Net-style [25] generator that enables real-time inference on high-resolution synthetic images. In addition, a hybrid training strategy that incorporates both the photorealism-enhanced pairs and matched patches from the real-world dataset that was utilized during the robust unpaired Im2Im translation is proposed to improve the visual realism and semantic consistency by avoiding learning the artifacts produced by the robust unpaired Im2Im translation model. The experimental results demonstrate that HyPER-GAN achieves lower inference latency, improved visual quality, and semantic consistency compared to State-of-The-Art (SoTA) paired Im2Im translation methods. Additionally, it is shown that the hybrid approach indeed improves the visual realism and the semantic robustness compared to training with a variation of HyPER-GAN, HyPER-GAN Enhanced Only (HyPER-GAN-EO), which employs only paired synthetic and photorealism-enhanced images.

Our contributions are summarized as follows:

- We propose HyPER-GAN, a lightweight paired Im2Im translation method for real-time photorealism enhancement of high-resolution synthetic images.
- We introduce a hybrid training strategy that combines paired synthetic–photorealism-enhanced image supervision with matched real-world image patches.
- We demonstrate through experiments that HyPER-GAN outperforms SoTA paired Im2Im translation methods in terms of inference latency, visual quality, and semantic consistency.
- We validate that the proposed hybrid training approach

leads to superior visual realism and semantic robustness compared to training solely with synthetic and photorealism-enhanced pairs.

II. HyPER-GAN

The HyPER-GAN method includes four phases as illustrated in Figure 1, namely the datasets and preprocessing, the real-world dataset indexing, the training, and the photorealism enhancement phases. These are detailed in the following subsections.

A. Datasets and Preprocessing

HyPER-GAN requires three types of datasets: (i) a synthetic dataset containing synthetic images (x) from simulators, e.g., CARLA [1] (see Appendix B) or video games, such as Grand Theft Auto V (GTA-V); (ii) a photorealism-enhanced dataset including photorealism-enhanced image pairs ($target$) of the synthetic dataset generated by a robust Im2Im model, such as Enhancing Photorealism Enhancement (EPE) [22], using real-world images as targets; and (iii) the real-world dataset that incorporates the real-world images ($real$) used as the target of realism during the robust unpaired Im2Im translation. All the images included in the datasets are preprocessed using the same pipeline. In detail, images are first resized to a fixed resolution of 512x512, which is a standard resolution employed by paired Im2Im translation methods such as Pix2PixHD [17]. Subsequently, each image is converted to a tensor and normalized using a mean and standard deviation of [0.5, 0.5, 0.5].

B. Real-World Dataset Indexing

To effectively incorporate real-world images in HyPER-GAN and considering the issues in unpaired Im2Im translation, where distributional object differences can result in visual artifacts since the discriminator will learn to distinguish real and generated images by these distribution differences [22], we follow a patch matching approach proposed in a previous photorealism enhancement unpaired Im2Im method (i.e., EPE). To this end, the Facebook AI Similarity Search (FAISS) [26] library is employed for fast nearest-neighbor search in high-dimensional spaces. In detail, we extract four 196×196 non-overlapping patches (after resizing to 512×512) from each *real* image of the real-world dataset (these patches are denoted as p^{real} in Figure 1) and subsequently compute feature embeddings $\phi(p^{real})$ for each patch using a pre-trained VGG-16 [27] backbone (the third convolutional layer in VGG-16 block 4), which are stored in the FAISS indexed database (\mathcal{R}) using L2 distance.

C. Training

Training follows the standard Generative Adversarial Network (GAN) process, where a generator (G) aims to generate photorealism-enhanced images, while a discriminator (D) attempts to classify whether an input image originates from the generator or the target domain dataset.

a) *Generator and Discriminator*: G is a lightweight U-Net-style network (an architecture widely employed for GANs [28], [29]), and D is a PatchGAN-style network operating on patches. In detail, G consists of an encoder (three down-sampling stages) and a decoder (three upsampling stages). The encoder receives a synthetic image $x \in \mathbb{R}^{3 \times H \times W}$ and progressively increases the feature dimensionality from 3 to 256 channels (64, 128, and 256) using strided convolutions. Instance normalization and ReLU activation are applied after all encoder layers, except for instance normalization after the first, as shown in Eq. 1.

$$\begin{aligned} e_1 &= \text{ReLU}(\text{Conv}_{4 \times 4}^{s=2, p=1}(x)) \\ e_2 &= \text{ReLU}(\text{IN}(\text{Conv}_{4 \times 4}^{s=2, p=1}(e_1))) \\ e_3 &= \text{ReLU}(\text{IN}(\text{Conv}_{4 \times 4}^{s=2, p=1}(e_2))) \end{aligned} \quad (1)$$

A bottleneck composed of four residual blocks enables deeper feature extraction while preserving spatial information through identity skip connections. In detail, each residual block contains two convolutional layers with instance normalization, using a ReLU activation after the first convolution and an identity skip connection as detailed in Eq. 2.

$$\begin{aligned} m &= \text{ResBlock}^{\times 4}(e_3) \\ \text{ResBlock}(z) &= z + \text{IN}(\text{Conv}_{3 \times 3}^{1,1}(\text{ReLU}(\text{IN}(\text{Conv}_{3 \times 3}^{1,1}(z)))))) \end{aligned} \quad (2)$$

The decoder mirrors the encoder using transposed convolutions and skip connections via feature concatenation from corresponding encoder stages. Instance normalization and ReLU activation are applied in intermediate decoder layers, and a final Tanh activation produces the normalized generated image $\hat{X} \in \mathbb{R}^{3 \times H \times W}$ as illustrated in Eq. 3

$$\begin{aligned} d_3 &= \text{ReLU}(\text{IN}(\text{ConvTranspose}_{4 \times 4}^{s=2, p=1}(m))) \\ d_2 &= \text{ReLU}(\text{IN}(\text{ConvTranspose}_{4 \times 4}^{s=2, p=1}([d_3 \| e_2]))) \\ G(x) = \hat{X} &= \text{Tanh}(\text{ConvTranspose}_{4 \times 4}^{s=2, p=1}([d_2 \| e_1])) \end{aligned} \quad (3)$$

where $[\cdot \| \cdot]$ denotes channel-wise concatenation.

The discriminator D follows a PatchGAN-style architecture that evaluates realism at the patch level. Given a patch $p \in \mathbb{R}^{3 \times H \times W}$, the D consists of a sequence of strided convolutional layers with increasing feature dimensionality (64, 128, and 256), progressively reducing spatial resolution while capturing local texture statistics, each followed by LeakyReLU activation. Instance normalization is applied to all layers except the first. A final 1×1 convolution outputs a single-channel feature map representing the realism scores of local image patches as presented in Eq. 4.

$$\begin{aligned} h_1 &= \text{LeakyReLU}_{0.2}(\text{Conv}_{4 \times 4}^{s=2, p=1}(p)) \\ h_2 &= \text{LeakyReLU}_{0.2}(\text{IN}(\text{Conv}_{4 \times 4}^{s=2, p=1}(h_1))) \\ h_3 &= \text{LeakyReLU}_{0.2}(\text{IN}(\text{Conv}_{4 \times 4}^{s=2, p=1}(h_2))) \\ D(p) &= \text{Conv}_{4 \times 4}^{s=1, p=1}(h_3) \end{aligned} \quad (4)$$

b) *Similarity Search*: For each generated image $\hat{X} = G(x)$, a set of four 196×196 non-overlapping patches \hat{p} is extracted. Subsequently, for every generated patch \hat{p} , the spatially corresponding patch p^{target} from the photorealism-enhanced image (*target*) pair is retrieved. To avoid learning artifacts from *target*, the FAISS indexed database is also employed to find (match) the nearest neighbor $p^{real} \in \mathcal{R}$ of \hat{p} in the VGG-16 feature space:

$$p^{mached} = \arg \min_{p^{real} \in \mathcal{R}} \|\phi(\hat{p}) - \phi(p^{real})\|_2^2 \quad (5)$$



Fig. 2. Examples of matched patches between the generated (top) and the real-world (bottom) patches.

Examples of such matched patches are illustrated in Figure 2, where it is evident that semantically similar content (e.g., sky, building, or advertisement board) is matched between the generated and the real-world images. Following the extraction of matched patches, we form two sets of batches that contain eight patches (since four patches are extracted from each image): a *generated* set $\mathcal{P}_{generated} = [\hat{p}, \hat{p}]$ and a *real* set $\mathcal{P}_{real} = [p^{target}, p^{mached}]$. By processing these sets of batches, D is forced to distinguish G 's output from both the enhanced (*target*) and the real-world (*real*)

domains. Particularly, this additional real-world supervision discourages G from learning artifacts introduced by the robust unpaired Im2Im translation network, as it must fool D not only on the photorealism-enhanced target domain but also on the real-world one, where such artifacts are absent. For comparison, we also consider a simplified variation, HyPER-GAN-EO, in which G is trained exclusively on the paired synthetic-photorealism-enhanced images ($\mathcal{P}_{generated} = [\hat{p}]$ and $\mathcal{P}_{real} = [p^{target}]$).

c) *Loss Functions*: G is trained using a combination of adversarial and reconstruction losses. The adversarial component follows the Least-Squares GAN (LSGAN) formulation [30], which replaces the binary cross-entropy objective with a least-squares loss to stabilize training and improve gradient quality. D is trained to assign a value of 1 to real patches \mathcal{P}_{real} and 0 to generated patches $\mathcal{P}_{generated}$. Conversely, G is trained to produce patches that are classified as real by D , i.e., to push $D(\mathcal{P}_{generated})$ toward 1. In addition, an L_1 reconstruction loss between the generated image \hat{X} and the photorealism-enhanced image $target$ is used to preserve structural and semantic consistency. The overall objectives are:

$$\begin{aligned}\mathcal{L}_D &= \mathbb{E}_{q \sim \mathcal{P}_{real}} [(D(q) - 1)^2] + \mathbb{E}_{q \sim \mathcal{P}_{generated}} [D(q)^2] \\ \mathcal{L}_G &= \mathbb{E}_{q \sim \mathcal{P}_{generated}} [(D(q) - 1)^2] + \lambda \|\hat{X} - target\|_1\end{aligned}\quad (6)$$

where $\lambda = 10$ is a weighting factor for L_1 distance.

D. Photorealism Enhancement

During the photorealism enhancement phase, HyPER-GAN operates as a standalone feed-forward network. In detail, the FAISS index and D are discarded, and given a synthetic input image x , the generator G directly produces the photorealism-enhanced output \hat{X} . HyPER-GAN does not require any additional input, such as G-Buffers or semantic segmentation maps that are typically required by robust unpaired Im2Im translation networks [22], [23], and therefore can be easily applied to any pre-existing synthetic dataset or output of a simulator [1].

III. EXPERIMENTS AND RESULTS

In this section, first, the experimental setup followed to illustrate the contributions of HyPER-GAN is detailed. Subsequently, the implementation details are outlined, and the results are presented and discussed.

A. Experimental Setup

The experimental setup involves the utilization of a dataset that was extracted from a virtual environment. To this end, the Playing for Data (PFD)¹ [31] dataset is employed. PFD includes a total of 25,000 individual synthetic images from the video game GTA-V at 1080p, accompanied by semantic segmentation annotations that follow the Cityscapes (CS) [32] annotation scheme. In addition, the photorealism-enhanced counterparts for a subset of 19,252 images of the PFD dataset, produced by EPE towards the characteristics of the

real-world datasets CS and Mapillary Vistas (MV) [33], are provided² in [22] and were used as the photorealism-enhanced pairs generated from a robust unpaired Im2Im translation method. In detail, in order to transform these datasets into a compatible dataset for paired Im2Im translation, the same 19,252 images from the synthetic PFD dataset were selected and resized to a resolution of 957×526 to match that of the photorealism-enhanced data. Subsequently, the 19,252 synthetic-photorealism-enhanced pairs were split using the official split provided by the authors, which results in 8,542 training, 4,453 validation, and 4,204 test images. Considering that the photorealism-enhanced pairs target the CS and MV real-world datasets, the images of these datasets were employed as the real-world images required by the proposed method. Specifically, we utilize the 5,000 images provided in the CS and the 25,000 included in MV.

Having constructed the required datasets, the HyPER-GAN and the HyPER-GAN-EO variation are trained to also learn to perform photorealism enhancement from the synthetic domain (GTA-V) towards the photorealism-enhanced outputs of EPE (CS and MV). The same training procedure is also performed for two baseline paired Im2Im translation methods, namely FastCUT [13] and REGEN [18]. Subsequently, the test set of the dataset is photorealism-enhanced with each of the trained models, and their visual quality is compared to the target real-world dataset (for example, images enhanced towards CS are evaluated against CS) using the Kernel Inception Distance (KID) [34] metric. To investigate the semantic preservation capabilities of the proposed HyPER-GAN, the HyPER-GAN-EO variation, and the baseline methods, Mask2Former [35] semantic segmentation models pretrained on the real-world datasets (i.e., CS and MV) using the official weights^{3,4} are also applied to the generated images, and their predictions are evaluated against the ground-truth label maps using Intersection over Union (IoU). A reduction in semantic segmentation accuracy compared to the one achieved with the initial synthetic images highlights that images generated by a certain method (HyPER-GAN, HyPER-GAN-EO, or the baselines) are subject to more visual artifacts and visual inconsistencies, such as hallucinations of objects. Since there are incompatibilities between the pretrained semantic segmentation models and the PFD dataset, we employ the typical 19 CS classes used for benchmarking semantic segmentation models [32] and set the remaining object classes as background.

B. Implementation Details

The HyPER-GAN and the HyPER-GAN-EO variation are implemented in PyTorch and trained on a single NVIDIA RTX 4070 Super GPU with 12GB of memory. G and D are optimized using the Adam optimizer with a learning rate of 2×10^{-4} and betas (0.5, 0.999). We train HyPER-GAN and HyPER-GAN-EO for 20 epochs with a batch size of 1. For REGEN, we use the official implementation⁵,

²<https://github.com/isl-org/PhotorealismEnhancement>

³<https://huggingface.co/facebook/mask2former-swin-tiny-cityscapes-semantic>

⁴<https://huggingface.co/facebook/mask2former-swin-large-mapillary-vistas-semantic>

⁵<https://github.com/stefanos50/REGEN>

¹https://download.visinf.tu-darmstadt.de/data/from_games/

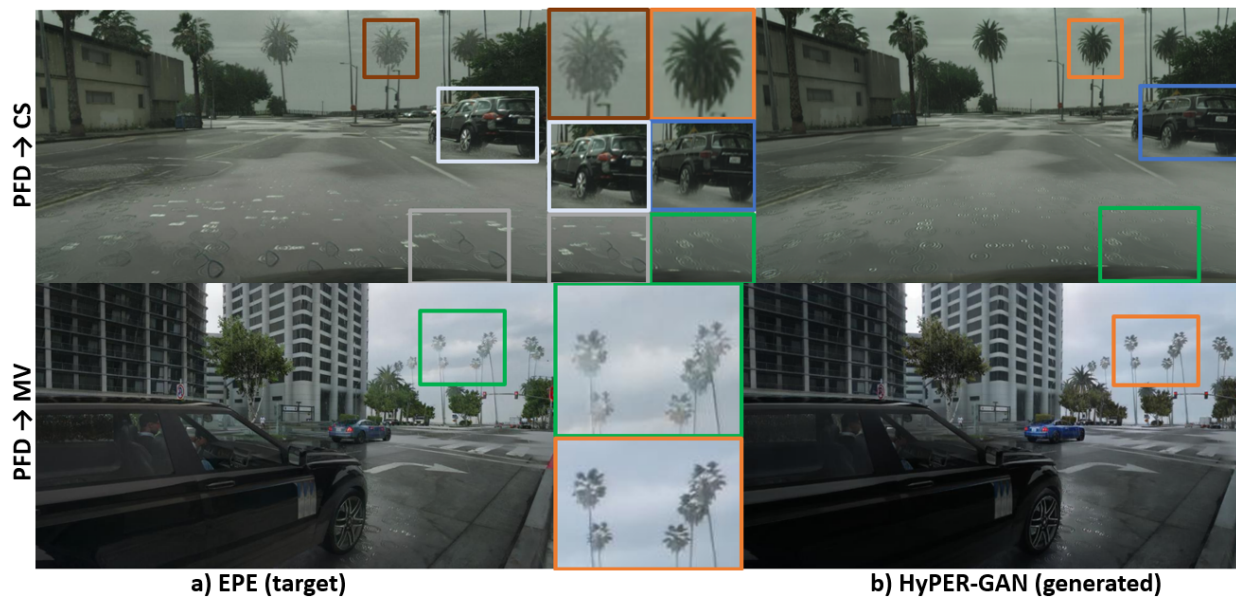


Fig. 3. Translation results of PFD (GTA-V) towards real-world datasets (CS and MV) produced by a) EPE and b) HyPER-GAN.

modifying only the preprocessing size to 512×512 , since the synthetic-photorealism-enhanced pairs have a resolution of 957×526 , which is smaller than the default resolution of 1024×512 . REGEN was trained for 9 epochs as in [18]. FastCUT was utilized with the implementation⁶ included in DCLGAN [14] with default parameters and was trained for 20 epochs. Regarding the real-time performance capabilities of the proposed HyPER-GAN and the baselines, Table I presents the inference latency and FPS, reported as mean \pm standard deviation over 100 images, as well as the VRAM utilization for FastCUT, REGEN, and HyPER-GAN. The HyPER-GAN-EO variation was not employed since it is based on the exact same generator G as HyPER-GAN. In detail, benchmarking was performed on a system equipped with an Intel i7-13700KF CPU, 32GB DDR4 RAM, and an NVIDIA RTX 4070 Super (12GB) GPU without any model compression or optimization (e.g., TensorRT). As demonstrated, the proposed framework achieves real-time performance, reaching the target 30 FPS at 1080p resolution with a mid-range GPU. Moreover, HyPER-GAN requires approximately half the VRAM of FastCUT and REGEN, making it significantly more accessible for deployment on consumer-grade hardware.

TABLE I
RUNTIME PERFORMANCE (LATENCY, FPS) AND VRAM USAGE OF
FASTCUT, REGEN, AND HYPER-GAN ACROSS DIFFERENT
RESOLUTIONS ON AN NVIDIA RTX 4070 SUPER GPU.

Model	Resolution	↓ Latency (ms)	↑ FPS	↓ VRAM (GB)
FastCUT	720p	128.210 ± 0.467	7.80 ± 0.032	2.3
	1080p	297.942 ± 3.516	3.36 ± 0.04	3.8
REGEN	720p	79.175 ± 0.770	12.63 ± 0.12	1.9
	1080p	180.973 ± 1.937	5.53 ± 0.06	3.1
HyPER-GAN	720p	12.347 ± 0.279	81.03 ± 1.80	0.8
	1080p	29.642 ± 0.175	33.74 ± 0.20	1.5

⁶<https://github.com/JunlinHan/DCLGAN>

C. Results and Discussion

In this subsection, we present the results of FastCUT, REGEN, HyPER-GAN-EO, and HyPER-GAN in terms of visual quality and semantic robustness. For reference, the metrics are also reported for the synthetic images of PFD. As shown in Table II, the photorealism-enhanced data generated by HyPER-GAN achieve lower KID values when compared to the respective real-world datasets than the ones produced by FastCUT, REGEN, and HyPER-GAN-EO. Moreover, the KID is significantly lower than the synthetic images of the PFD dataset. Particularly, the most significant improvement of visual realism is observed for the CS dataset, demonstrating that the proposed hybrid approach effectively enhances photorealism. In addition to the improved visual realism manifested by lower KID, the Mask2Former pretrained models manage to achieve the highest segmentation accuracy on the photorealism-enhanced images produced by HyPER-GAN, reaching close to the one achieved on synthetic images (PFD) for the CS translated images. This indicates that the proposed method enhances photorealism without compromising the semantic integrity of the initially synthetic scenes compared to the baselines, which are subject to more artifacts.

These observations are further illustrated in Figure 3, which compares the outputs of HyPER-GAN with the *target* domain produced by the robust unpaired image-to-image (Im2Im) translation method (i.e., EPE). In detail, EPE often introduces artifacts, including hallucinated vegetation, geometric distortions in water surfaces, and unrealistic glossiness on vehicles, even under low-light conditions. HyPER-GAN, leveraging supervision from matched patches in the real-world domain, avoids learning these artifacts. In contrast, FastCUT and REGEN, which lack this mechanism, remain prone to unrealistic glossiness and hallucinations, as illustrated in Figure 4.

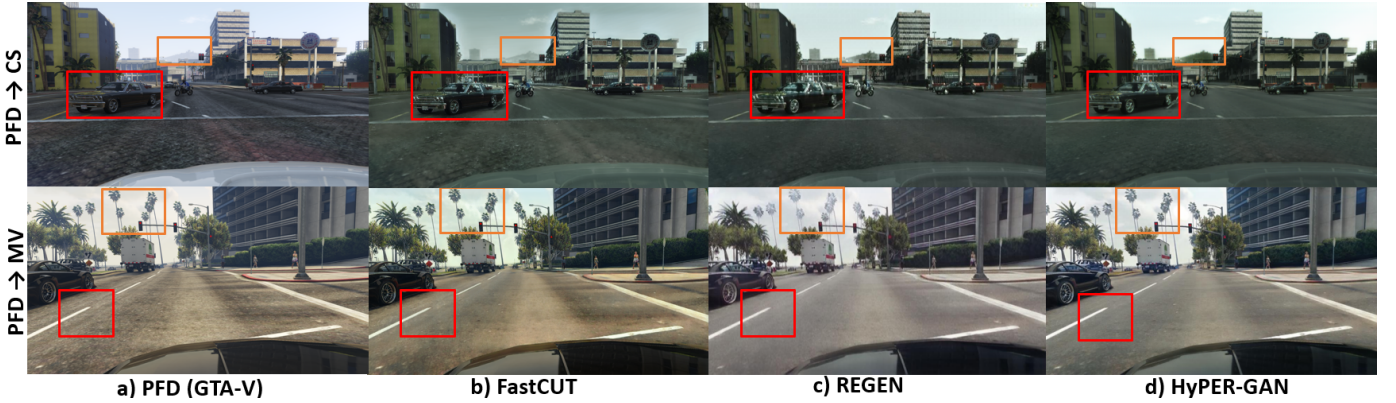


Fig. 4. Translation results of PFD (GTA-V) towards the real-world datasets CS and MV produced by a) FastCUT, b) REGEN, and c) HyPER-GAN.

TABLE II

VISUAL REALISM AND SEMANTIC ROBUSTNESS EVALUATION ON THE PHOTOREALISM-ENHANCED DATA PRODUCED BY HYPER-GAN, THE HYPER-GAN-EO VARIATION, AND THE BASELINES, USING KID AND MIOU, RESPECTIVELY.

Method	CS		MV	
	↓ KID $\times 100$	↑ mIoU	↓ KID $\times 100$	↑ mIoU
PFD	7.98	49.09%	4.47	61.09%
FastCUT	4.55	46.75%	3.04	58.97%
REGEN	3.94	46.02%	2.52	56.54%
HyPER-GAN-EO	4.06	47.04%	2.61	59.01%
HyPER-GAN	3.41	48.79%	2.39	59.13%

IV. CONCLUSION

In this paper, we presented HyPER-GAN, a lightweight paired Im2Im translation method for real-time photorealism enhancement of synthetic data. By combining an efficient U-Net-style generator with a hybrid training strategy that incorporates matched real-world patches, HyPER-GAN achieves improved visual realism and semantic consistency while meeting real-time performance constraints. The experimental results demonstrated that the proposed method outperforms existing paired Im2Im methods in both visual quality and semantic robustness, making it suitable for real-time and large-scale synthetic data photorealism enhancement. Through a variation of the method, HyPER-GAN-EO, it was also illustrated that the hybrid training approach indeed improves the visual quality and semantic consistency.

APPENDIX A

COMPARISON WITH A DIFFUSION MODEL

In this appendix, we compare HyPER-GAN and REGEN (which provided the best visual results in Section III-C) with a SoTA diffusion-based model. In detail, we compare with COSMOS Transfer1 (edge distilled with a control weight of 1.0)⁷ [11] using the validation videos 01–19 of the Playing for Benchmark (PFB)⁸ dataset [36] (since COSMOS Transfer1 can be applied only on videos). For HyPER-GAN and REGEN models trained to translate PFD towards CS are employed. Visual realism is evaluated using KID against the MV dataset

(since COSMOS Transfer1 isn’t trained to specifically enhance the photorealism towards CS), while semantic preservation is evaluated using a pretrained YOLOv12 [37] detector pre-trained on Common Objects in Context (COCO) [38] over six objects: car, motorbike, bus, truck, person, and traffic light. As shown in Table III, HyPER-GAN achieves better visual realism and preserves semantics more effectively than both REGEN and COSMOS Transfer1, with the latter frequently producing artifacts or hallucinating objects as shown in Figure 5.

TABLE III

VISUAL REALISM (KID) AND SEMANTIC ROBUSTNESS (MAP) EVALUATION ON THE PHOTOREALISM-ENHANCED DATA PRODUCED BY REGEN, COSMOS TRANSFER1, AND HYPER-GAN ON PFB.

Method	↓ KID $\times 100$	↑ mAP@50	↑ mAP@50–95
PFB	7.69	25.72%	17.31%
REGEN	6.69	21.70%	14.13%
COSMOS Transfer1	8.39	14.00%	8.76%
HyPER-GAN	6.50	22.15%	14.67%

APPENDIX B

CROSS-ENGINE EVALUATION ON A SIMULATOR

In this appendix, we evaluate the generalization capability of HyPER-GAN on CARLA-UE5, a dataset⁹ extracted from the Unreal Engine 5 version of the CARLA simulator [39]. The model, trained to translate PFD to CS, is applied to this dataset and compared with REGEN and EPE, which were trained on images from the Unreal Engine 4 version of CARLA (CARLA-UE4) [7] for translation towards CS. The pretrained models are provided in [7] for EPE and [18] for REGEN. As shown in Table IV, HyPER-GAN outperforms EPE (in terms of KID), which has poor generalization, and achieves competitive visual quality and semantic preservation compared to REGEN, despite being trained on PFD (GTA-V), which is based on a different game engine (RAGE for GTA-V and Unreal Engine for CARLA) with unseen assets and environments. As shown in Figure 6, HyPER-GAN improves the photorealism of the CARLA simulator, especially on the

⁷<https://github.com/nvidia-cosmos/cosmos-transfer1>

⁸<https://playing-for-benchmarks.org/download/>

⁹<https://www.kaggle.com/datasets/stefanospasios/carla2realue5-enhancing-photorealism-in-carla-ue5>

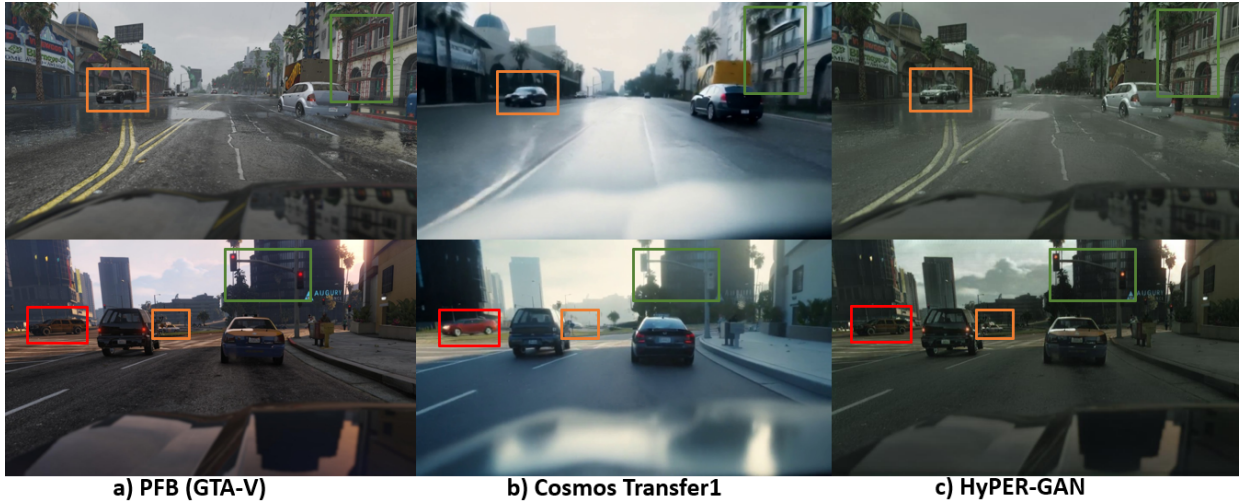


Fig. 5. Comparison of images generated by (b) COSMOS Transfer1 and (c) HyPER-GAN, given as input an image (a) from the PFB dataset.



Fig. 6. Photorealism-enhanced image (right) produced by HyPER-GAN given a synthetic image from the CARLA (Unreal Engine 5) simulator (left).



Fig. 7. Photorealism-enhanced image (right) produced by HyPER-GAN given a synthetic image from Resident Evil Requiem (left).

texture of the road. In addition, a qualitative cross-engine result is provided for HyPER-GAN trained to translate PFD towards the characteristics of CS applied on the recently released video game Resident Evil Requiem. As illustrated in Figure 7, despite the game being unseen during training, the model successfully translates the scene and adapts visual elements such as clothing textures, even though it was trained exclusively on outdoor urban scenes captured from GTA-V.

REFERENCES

- [1] A. Dosovitskiy, G. Ros, F. Codevilla, A. Lopez, and V. Koltun, “Carla: An open urban driving simulator,” 2017.

TABLE IV
VISUAL REALISM AND SEMANTIC ROBUSTNESS EVALUATION ON THE PHOTOREALISM-ENHANCED DATA PRODUCED BY REGEN, EPE, AND HYPER-GAN, USING KID AND MIOU, RESPECTIVELY.

Method (Trained)	CS	
	↓ KIDx100	↑ mIoU
CARLA-UE5	5.53	34.84%
REGEN (CARLA-UE4)	4.25	29.06%
EPE (CARLA-UE4)	5.88	33.65%
HyPER-GAN (PFD)	4.40	29.52%

- [2] S. Shah, D. Dey, C. Lovett, and A. Kapoor, "Airsim: High-fidelity visual and physical simulation for autonomous vehicles," 2017. [Online]. Available: <https://arxiv.org/abs/1705.05065>
- [3] G. Rong, B. H. Shin, H. Tabatabaee, Q. Lu, S. Lemke, M. Možeiko, E. Boise, G. Uhm, M. Gerow, S. Mehta, E. Agafonov, T. H. Kim, E. Sterner, K. Ushiroda, M. Reyes, D. Zelenkovsky, and S. Kim, "Lgsvl simulator: A high fidelity simulator for autonomous driving," in *2020 IEEE 23rd International Conference on Intelligent Transportation Systems (ITSC)*, 2020, pp. 1–6.
- [4] Q. Wang, J. Gao, W. Lin, and Y. Yuan, "Learning from synthetic data for crowd counting in the wild," in *Proceedings of IEEE Conference on Computer Vision and Pattern Recognition (CVPR)*, 2019, pp. 8198–8207.
- [5] S. Pasiros, K. Gkountakos, K. Ioannidis, T. Tsikrika, S. Vrochidis, and I. Kompatsiaris, "Photorealistic synthetic crowds simulation in indoor environments (pacs-i): a novel synthetic dataset for realistic simulation of crowd panic and violence behaviors," *IEEE Access*, pp. 1–1, 2025.
- [6] M. Kästingschäfer, T. Gieruc, S. Bernhard, D. Campbell, E. Insafutdinov, E. Najafii, and T. Brox, "Seed4d: A synthetic ego-exo dynamic 4d data generator, driving dataset and benchmark," in *2025 IEEE/CVF Winter Conference on Applications of Computer Vision (WACV)*, 2025, pp. 7752–7764.
- [7] S. Pasiros and N. Nikolaidis, "Carla2real: A tool for reducing the sim2real appearance gap in carla simulator," *IEEE Transactions on Intelligent Transportation Systems*, vol. 26, no. 11, pp. 18747–18761, 2025.
- [8] N. Gadipudi, I. Elamvazuthi, M. Sanmugam, L. I. Izhar, T. Prasetyo, R. Jegadeeswaran, and S. S. A. Ali, "Synthetic to real gap estimation of autonomous driving datasets using feature embedding," in *2022 IEEE 5th International Symposium in Robotics and Manufacturing Automation (ROMA)*, 2022, pp. 1–5.
- [9] C. Samak, T. Samak, B. Li, and V. Krovi, "Sim2real diffusion: Leveraging foundation vision language models for adaptive automated driving," *IEEE Robotics and Automation Letters*, vol. 11, no. 1, pp. 177–184, 2026.
- [10] H. Hoyez, C. Schockaert, J. Rambach, B. Mirbach, and D. Stricker, "Unsupervised image-to-image translation: A review," *Sensors*, vol. 22, no. 21, 2022.
- [11] H. A. Alhaija *et al.*, "Cosmos-transfer1: Conditional world generation with adaptive multimodal control," 2025.
- [12] L. Zhang, A. Rao, and M. Agrawala, "Adding conditional control to text-to-image diffusion models," in *2023 IEEE/CVF International Conference on Computer Vision (ICCV)*, 2023, pp. 3813–3824.
- [13] T. Park, A. A. Efros, R. Zhang, and J.-Y. Zhu, "Contrastive learning for unpaired image-to-image translation," 2020.
- [14] J. Han, M. Shoenby, L. Petersson, and M. A. Armin, "Dual contrastive learning for unsupervised image-to-image translation," in *2021 IEEE/CVF Conference on Computer Vision and Pattern Recognition Workshops (CVPRW)*, 2021, pp. 746–755.
- [15] J. D. Theiss, J. Leverett, D. Kim, and A. Prakash, "Unpaired image translation via vector symbolic architectures," in *European Conference on Computer Vision*, 2022.
- [16] S. Xie, Y. Xu, M. Gong, and K. Zhang, "Unpaired image-to-image translation with shortest path regularization," in *2023 IEEE/CVF Conference on Computer Vision and Pattern Recognition (CVPR)*, 2023, pp. 10177–10187.
- [17] T.-C. Wang, M.-Y. Liu, J.-Y. Zhu, A. Tao, J. Kautz, and B. Catanzaro, "High-resolution image synthesis and semantic manipulation with conditional gans," in *2018 IEEE/CVF Conference on Computer Vision and Pattern Recognition*, 2018, pp. 8798–8807.
- [18] S. Pasiros and N. Nikolaidis, "Regen: Real-time photorealism enhancement in games via a dual-stage generative network framework," *IEEE Transactions on Games*, pp. 1–8, 2026.
- [19] T. R. Shaham, M. Gharbi, R. Zhang, E. Shechtman, and T. Michaeli, "Spatially-adaptive pixelwise networks for fast image translation," in *2021 IEEE/CVF Conference on Computer Vision and Pattern Recognition (CVPR)*, 2021, pp. 14877–14886.
- [20] S. Suri, M. Meshry, L. S. Davis, and A. Shrivastava, "Grit: Gan residuals for paired image-to-image translation," in *2024 IEEE/CVF Winter Conference on Applications of Computer Vision (WACV)*, 2024, pp. 4953–4963.
- [21] J. Pahk, J. Shim, M. Baek, Y. Lim, and G. Choi, "Effects of sim2real image translation via dclgan on lane keeping assist system in carla simulator," *IEEE Access*, vol. 11, pp. 33915–33927, 2023.
- [22] S. R. Richter, H. A. Alhaija, and V. Koltun, "Enhancing photorealism enhancement," *IEEE Transactions on Pattern Analysis and Machine Intelligence*, vol. 45, no. 2, pp. 1700–1715, 2023.
- [23] E. Ioannou and S. Maddock, "Toward real-time g-buffer-guided style transfer in computer games," *IEEE Transactions on Games*, vol. 17, no. 3, pp. 613–621, 2025.
- [24] G. Eskandar, D. Guo, K. Guirguis, and B. Yang, "Towards pragmatic semantic image synthesis for urban scenes," in *2023 IEEE Intelligent Vehicles Symposium (IV)*, 2023, pp. 1–8.
- [25] O. Ronneberger, P. Fischer, and T. Brox, "U-net: Convolutional networks for biomedical image segmentation," in *Medical Image Computing and Computer-Assisted Intervention – MICCAI 2015*, N. Navab, J. Hornegger, W. M. Wells, and A. F. Frangi, Eds. Cham: Springer International Publishing, 2015, pp. 234–241.
- [26] M. Douze, A. Guzhva, C. Deng, J. Johnson, G. Szilvasy, P.-E. Mazaré, M. Lomeli, L. Hosseini, and H. Jégou, "The faiss library," *IEEE Transactions on Big Data*, pp. 1–17, 2025.
- [27] S. Liu and W. Deng, "Very deep convolutional neural network based image classification using small training sample size," in *2015 3rd IAPR Asian Conference on Pattern Recognition (ACPR)*, 2015, pp. 730–734.
- [28] E. Batziou, K. Ioannidis, I. Patras, S. Vrochidis, and I. Kompatsiaris, "Hdd-unet: A unet-based architecture for low-light image enhancement," *Image and Vision Computing*, vol. 167, p. 105889, 2026.
- [29] E. Schönfeld, B. Schiele, and A. Khoreva, "A u-net based discriminator for generative adversarial networks," in *2020 IEEE/CVF Conference on Computer Vision and Pattern Recognition (CVPR)*, 2020, pp. 8204–8213.
- [30] X. Mao, Q. Li, H. Xie, R. Y. Lau, Z. Wang, and S. P. Smolley, "Least squares generative adversarial networks," in *2017 IEEE International Conference on Computer Vision (ICCV)*, 2017, pp. 2813–2821.
- [31] S. R. Richter, V. Vineet, S. Roth, and V. Koltun, "Playing for data: Ground truth from computer games," 2016.
- [32] M. Cordts, M. Omran, S. Ramos, T. Rehfeld, M. Enzweiler, R. Benenson, U. Franke, S. Roth, and B. Schiele, "The cityscapes dataset for semantic urban scene understanding," in *2016 IEEE Conference on Computer Vision and Pattern Recognition (CVPR)*, 2016, pp. 3213–3223.
- [33] G. Neuhold, T. Ollmann, S. R. Bulò, and P. Kotschieder, "The mapillary vistas dataset for semantic understanding of street scenes," in *2017 IEEE International Conference on Computer Vision (ICCV)*, 2017, pp. 5000–5009.
- [34] M. Bińkowski, D. J. Sutherland, M. Arbel, and A. Gretton, "Demystifying mmd gans," 2021.
- [35] B. Cheng, I. Misra, A. G. Schwing, A. Kirillov, and R. Girdhar, "Masked-attention mask transformer for universal image segmentation," in *2022 IEEE/CVF Conference on Computer Vision and Pattern Recognition (CVPR)*, 2022, pp. 1280–1289.
- [36] S. R. Richter, Z. Hayder, and V. Koltun, "Playing for benchmarks," in *IEEE International Conference on Computer Vision, ICCV 2017, Venice, Italy, October 22-29, 2017*, 2017, pp. 2232–2241.
- [37] Y. Tian, Q. Ye, and D. Doermann, "Yolov12: Attention-centric real-time object detectors," *arXiv preprint arXiv:2502.12524*, 2025.
- [38] T.-Y. Lin, M. Maire, S. Belongie, J. Hays, P. Perona, D. Ramanan, P. Dollár, and C. L. Zitnick, "Microsoft coco: Common objects in context," in *Computer Vision – ECCV 2014*, D. Fleet, T. Pajdla, B. Schiele, and T. Tuytelaars, Eds. Cham: Springer International Publishing, 2014, pp. 740–755.
- [39] S. Pasiros and N. Nikolaidis, "Enhancing photorealism in carla autonomous driving simulator," in *2025 33rd European Signal Processing Conference (EUSIPCO)*, 2025, pp. 671–675.